Available online www.jsaer.com

***Journal of Scientific and Engineering Research*, 2025, 12(2):15-24**

Research Article

ISSN: 2394-2630
CODEN(USA): JSERBR

Determination of Land Surface Temperature (LST) with Landsat 8: Application of Tekirdag - Sarkoy Region

Selçuk ALBUT[1*], Tulin Tuanna TURKOGLU[2]

[1]TNKU, Agriculture Faculty, Dept. of Biosystem Eng., Tekirdag, Turkiye
[2]TNKU, Agriculture Faculty, Dept. of Biosystem Eng., Graduate Student, Tekirdag, Turkiye

Abstract: Land Surface Temperature (LST) denotes the thermodynamic temperature of the Earth's surface, characterized by the radiative temperature emitted from that surface. It offers insights into surface energy fluxes and atmospheric interactions. Land Surface Temperature (LST) displays considerable diversity in regional and temporal dimensions, due to diverse climatic factors, land cover, soil and vegetation moisture levels, surface radiative properties, and topographical characteristics. Satellite data has advantages over situ measurements, such as global accessibility, consistency, and geographically distributed data collecting, leading to a cost-effective and efficient data stream. LST is widely employed in several fields, including agriculture, phenological development, planting depth recommendations, yield forecasting models, weather and climate monitoring, heatwave assessment, urban island effect study, and environmental impact assessment. Determining Land Surface Temperature (LST) using Landsat 8 thermal bands requires image preprocessing, rectification, geocoding, and analysis. Vegetation and emitted radiation are critical for determining land surface temperature (LST).

Keywords: Land Surface Temperature (LST), Land surface emissivity (LSE), NDVI, Remote Sensing, QGIS

1. Introduction

Global warming and climate change, critical environmental challenges confronting the planet, have begun to manifest their effects more aggressively in recent years. This issue endangers agricultural territories, forests, and available clean water resources, largely affecting biodiversity, but also contributing to rising sea levels [1]. Latent heat storage is a fundamental component of Earth's climate and several physical, chemical, and biological processes. Given that climate change is a global warming phenomenon, it is essential to utilize space technology for the monitoring of land surface temperature (LST). Urban warming includes an additional phenomenon referred to as the urban heat island effect. Land surface temperature correlates with several biophysical and demographic parameters, requiring that quantitative assessments account for this relationship.

Currently, urbanization results in elevated temperatures in densely inhabited regions compared to rural ones. Materials like asphalt and concrete used in roadways, roofs, walkways, and building structures absorb and retain more solar radiation than natural surfaces.

Surface temperature is a critical element in the domains of global energy equilibrium, perspiration and evaporation, aridity, global transformation, and urban heat islands [3]. Surface temperature (ST) refers to the temperature emitted from the Earth's surface, mostly derived from solar radiation. Solar energy that reaches the Earth's surface is transformed into thermal energy, elevating the temperature of things. Certain materials employed in urbanization and building absorb energy instead of reflecting it, thereby exacerbating the Urban Heat Island (UHI) effect [2].

Land surface temperature, extensively utilized across several fields, is a crucial metric that influences surface energy flows. Typical applications of LST encompass soil moisture assessment, forest fire detection, urban heat island monitoring, hydrological process investigations, and climate research [4].

The surface albedo, as a component of the surface radiation stack, is a crucial parameter for diagnosing surface conditions, significantly influencing the interaction between sensible and latent heat fluxes [5].

LST data is a crucial element often utilized in analyses and studies, including vegetation change analysis, land use and land cover change assessments, global warming research, and meteorological investigations [2]. The methodologies for acquiring LST have been created based on several data sources. The predominant methods utilized are the split-window technique, the temperature/emissivity separation method, the mono-window approach, and the single channel method [3].

Remote sensing measurements provide the most efficient method for monitoring land surface temperature across extensive regions and at regular intervals. The majority of satellite remote sensing products rely on data inside the thermal infrared (IR) atmospheric window, namely in the 8-13 μm range [4]. Satellite-derived data serve as a resource in several applications owing to its cost-effectiveness and extensive coverage. Landsat 8, a remote sensing platform deployed in 2013, is the most recent addition to the Landsat program, one of NASA's longest-running aerospace initiatives. It supplies users with data via its two thermal bands and nine spectral bands [2].

Assessing the association between alterations in land use and land surface temperature across extensive regions without employing remote sensing is very challenging. The advent of satellite-derived thermal imagery enables the acquisition of temporal surface temperature variations and the comparison of land use and land cover changes. The identification of surface temperature variations with remote sensing data predominantly use Landsat TM/ETM+, MODIS (Moderate Resolution Imaging Spectroradiometer), AVHRR (Advanced Very High Resolution Radiometer), and SPOT sensors [6].

Şekertekin et al. indicated that three distinct approaches are often employed to derive surface temperature from Landsat 5 TM data: the radiative transfer equation, the single window algorithm, and the single channel algorithm. They asserted that the single window technique outperforms the single channel algorithm, exhibiting a root mean square error of 0.9 Kelvin (ºK).

The Land Surface Temperature (LST) represents the thermodynamic temperature of the Earth's surface and characterizes the radiative temperature radiated by that surface, offering insights into surface energy fluxes and atmospheric interactions [7]. The data presented illustrates the temperature as perceived from a satellite's viewpoint. The "surface" denotes what the sensor perceives when seeing the ground through the atmosphere, including the canopy top in forested regions, soil in barren areas, or roofs in urban environments. Thus, Land Surface Temperature diverges from the air temperature shown in daily weather forecasts. LST provides insights into several applications, including evaporation monitoring, climate change research, soil moisture evaluation, vegetation analysis, and urban studies, among others [8], [9], [10], [11], [12].

The Land Surface Temperature may be assessed with the thermal bands of Landsat 8. It requires the implementation of many equations using a raster image calculator using QGIS.

This study illustrates the computation of Land Surface Temperature (LST) utilizing the bands of Landsat 8. Band 10 functions as the temperature band, whereas bands 4 and 5 are employed to calculate the Normalized Difference Vegetation Index (NDVI). LST is the radiative skin temperature of the Earth's surface derived from solar radiation. It is a crucial element affecting terrestrial thermal dynamics, since it governs the effective radiating temperature of the Earth's surface. LST is linked to several aspects of geoscience, rendering the understanding of its evolution and worldwide distribution essential for monitoring climate change, crop management, land cover changes, and various other uses [12], [13], [14].

Obtaining LST requires picture preparation, correction of distortions from satellite image capture, assessment of geometric and temporal alignment with other data sources via geocoding and projection onto an appropriate system, followed by image analysis. Sensors measure digital data that must be transformed into radiance and then into brightness temperature using recognized methods. Vegetation is a crucial factor influencing land surface temperature. Brightness temperature is employed to calculate the Normalized Difference plant Index (NDVI), a measure of plant greenness. The computation of NDVI enables the assessment of the proportion of plant cover in the designated area. The last component in determining Land Surface Temperature (LST) is Land Surface Emissivity, utilized to evaluate emitted radiance based on soil, vegetation, and surface roughness

parameters. These variables allow the capture of land surface temperature at the spatial resolution provided by the sensors [15].

2. Materials and Methods

Research Area

Tekirdag is one of the three cities located in the northwest of the Sea of Marmara, situated on the European continent, characterized by a relatively flat terrain and richer alluvial soil. The Tekirdağ province and Şarköy district, prominent regions for winemaking in Thrace, have been selected as the study site (Fig. 1). The overall area of Tekirdağ province is 6,313 km², whereas the total area of Şarköy district is 555 km².

The Tekirdağ province is situated between the longitudes of 26˚43' and 28˚08' east, and the latitudes of 40˚36' and 41˚31' north. It is bordered by Istanbul to the east, Edirne and Çanakkale to the west, the Sea of Marmara to the south, and Kırklareli to the north, with a little coastline along the Black Sea.

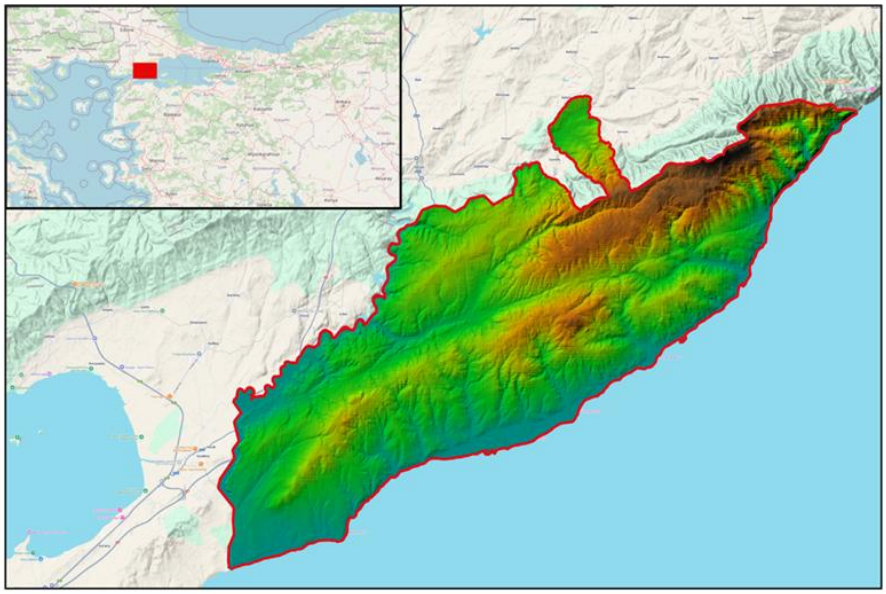

Figure 1: Tekirdag province and Sarkoy district

Data Collection

The Landsat 8 image, captured by the Operational Land Imager, depicting the northwestern area of Turkey, was sourced from the United States Geological Survey Earth Explorer's complimentary online data services for land surface temperature analysis [17]. The image was acquired with under 10% cloud cover in June 2024 (Table 1).

Table 1: Landsat imagery utilized for the Land Surface Temperature mapping of Tekirdag

LANDSAT SCENE ID	Sensor	Resolution	Path/Row	Date
LC81810322024153LGN00	Landsat 8	30 m	181/032	06.01.2024

Image Processing and Rectifications

Three operations were performed to process the image. These include coordinate reference processing, including image preparation and correction. In image pre-processing, both visual and digital image processing were performed, following the loading of images into QGIS 3.34 software for further processing. Thermal Infrared Band 10 was chosen for further analysis.

Image rectifications were performed to correct data distortion that may have resulted from the image acquisition process, employing the Impact toolbox developed by the European Union Joint Research Centre. To provide accurate identification of temporal fluctuations and geometric congruence with other informative sources, image was geocoded to the coordinate and mapping system of the national topographic maps. The image was projected onto the Universal Transverse Mercator (UTM) coordinate system, zone 35 North.

Image Analysis

The technique was developed in QGIS 3.34. This study utilized Landsat 8's Thermal Infrared band (Band 10) to estimate brightness temperatures, whereas bands 4 (Red) and 5 (Infrared) were employed to calculate the NDVI. The LST retrieval algorithms were obtained from the USGS website for acquiring top of atmospheric (TOA) spectral radiance [18]. The LST was obtained by adhering to the procedures outlined in Figure 2.

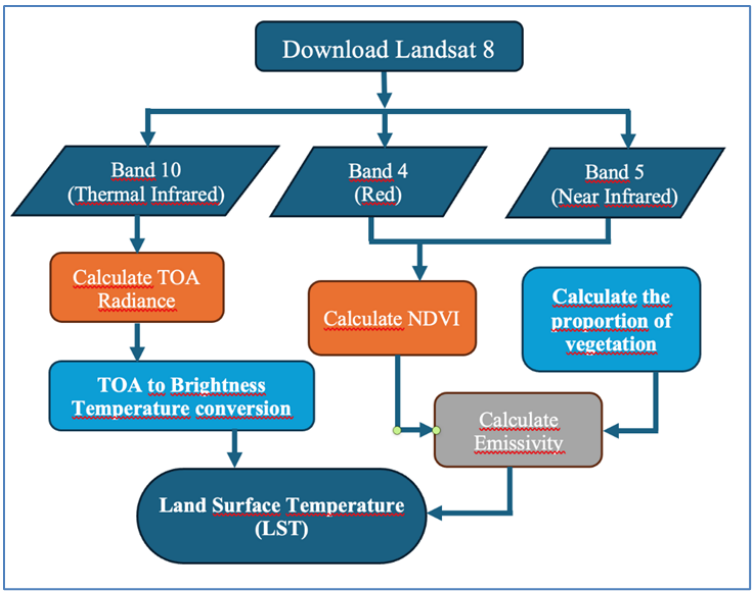

Figure 2: Flowchart for LST processing.

Calculation of TOA (Top of Atmospheric)

Top of Atmosphere (TOA) Reflectance is a dimensionless metric that indicates the ratio of reflected radiation to the incident solar radiation on a certain surface. It may be calculated using satellite-measured spectral radiance utilizing the mean solar spectral irradiance and the solar zenith angle [19]. Landsat Level-1 data may be transformed into TOA spectral radiance utilizing the radiance rescaling variables found in the MTL file. The equations' information is located in the Text documentation within the Landsat 8 data folder obtained from the U.S. Geological Survey EarthExplorer website.

$$L_\lambda = M_L\, Q_{cal} + A_L \quad (1)$$

where:

L_λ = TOA spectral radiance (Watts/(m^2 * srad * μm))

M_L =Band-specific multiplicative rescaling factor from the metadata,

A_L=Band-specific additive rescaling factor from the metadata

Q_{cal} = Quantized and calibrated standard product pixel values (DN).

The Raster Calculator feature in the QGIS program is utilized to compute this equation.

Conversion TOA to Brightness Temperature

Thermal band data can be transformed from spectral radiance to top of atmospheric brightness temperature utilizing the thermal constants included in the MTL file:

$$B_T = \frac{K_2}{ln\left(\frac{K_1}{L_\lambda}\right)+1} - 273.15 \quad (2)$$

where:

B_T = Top of atmosphere brightness temperature (K)

L_λ =TOA spectral radiance (Watts/(m2 * srad * μm))

K_1 = Band-specific thermal conversion constant from the metadata

K_2 = Band-specific thermal conversion constant from the metadata

Consequently, to derive the values in Celsius, the radiant temperature is modified by include absolute zero (about -273.15°C). The satellite data products constituted a geometrically adjusted dataset. Table 2 presents the information of the satellite pictures.

Table 2: Metadata of the Landsat 8 images

Metadata Variable	Description	Value
M_L	RADIANCE MULT BAND 10	0.0003342
A_L	RADIANCE ADD BAND 10)	0.10000
K_1	CONSTANT BAND 10	774.8853
K_2	CONSTANT BAND 10	1321.0789

Calculate the NDVI

The normalized differences vegetation index (NDVI), obtained from remote-sensing satellite data, is strongly associated with drought conditions. To ascertain the density of greenery on a parcel of land, the specific colors (wavelengths) of visible and near-infrared sunlight reflected by the vegetation are analyzed; the red and near-infrared bands, namely Band 4 and Band 5, were employed for computing the Normalized Difference Vegetation Index (NDVI). Estimating the NDVI is crucial, as the extent of vegetation is a significant influence, and NDVI serves to estimate overall vegetation health. The computation of the NDVI is crucial since it subsequently enables the calculation of the proportion of vegetation (PV), which is closely associated with the NDVI, and the emissivity (ε), which is linked to the PV.

$$NDVI = \frac{NIR(Band\ 5) - Red\ (Band\ 4)}{NIR(Band\ 5) + Red\ (Band\ 4)} \quad (3)$$

Where, NIR represents the near-infrared band (Band 5) and R represents the red band (Band 4). The data in this equation were calculated using the Raster Calculator using bands 4 and 5 of the Landsat 8 satellite image.

Calculate the proportion of vegetation

The Vegetation Fraction is defined as the fraction of ground area occupied by vegetation in vertical projection. Alterations in vegetation cover immediately influence surface water and energy budgets via plant transpiration, surface albedo, emissivity, and roughness. The proportion of vegetation (PV) is closely associated with NDVI values for both vegetation and soil. In this work, PV was assessed using the conventional NDVI approach [20], [21].

$$P_v = \left(\frac{NDVI - NDVI_{min}}{NDVI_{max} - NDVI_{min}}\right)^2 \quad (4)$$

Where $NDVI_v$ and $NDVI_s$ are Maximum and Minmum NDVI respectively representing NDVI of Vegetation and NDVI of soil respectively (in our application, the minimum value is calculated as -0.26334 and the maximum value is calculated as 0.653719).

The formula for calculating the proportion of vegetation (Pv) is executed using the Raster Calculator tool as outlined, and the procedure is carried out.

$$P_v = (("NDVI@1" - 0.26334) / (0.653719 - 0.26334))\ \hat{}\ 2 \quad (5)$$

The minimum and maximum values of the NDVI image are often presented directly inside the image; otherwise, one must access the raster attributes to obtain those values.

Calculate the land surface emissivity

The emissivity (ε) values for the land cover classes are presented in the subsequent table (the values utilized in this tutorial are only illustrative, since the emissivity of each material should be determined by field surveys) [22], [23].

Land Surface Emissivity (LSE). Average emissivity of a surface element of the Earth derived from observed radiance and land surface temperature. To determine land surface temperature (LST), it is essential to ascertain the land surface emissivity (LSE (ε)), since the LSE serves as a proportionality factor that correlates blackbody

radiation with emitted radiance, reflecting the efficiency of thermal energy transmission from the surface to the atmosphere. The ground emissivity is conditionally estimated as proposed in references [24], [25], and [26].

$$\varepsilon_\lambda = \varepsilon_{V\lambda} P_V + \varepsilon_{S\lambda}(1 - P_V) + C_\lambda \quad (6)$$

Where; ε_v and ε_s are the vegetation and soil emissivities respectively, and C is the surface roughness taken as a constant value of 0.005. The emissivity of aquatic bodies is far more steady than that of terrestrial surfaces. The NDVI threshold technique (NTM) can measure the emissivity of various terrestrial surfaces in the 10-12 μm region, as emissivity is wavelength-dependent. The spectral range of Band 10 of Landsat 8 is appropriate within this range. Within this wavelength range, the emissivity can be represented as follows [22]:

$$\varepsilon_\lambda = \begin{cases} \varepsilon_{S\lambda}, & NDVI < NDVI_S \\ \varepsilon_{V\lambda} P_V + \varepsilon_{S\lambda}(1 - P_V) + C_\lambda, & NDVI_S \le NDVI \le NDVI_V \\ \varepsilon_{V\lambda} P_V + C_\lambda, & NDVI > NDVI_{VS} \end{cases} \quad (7)$$

Table 3 presents the discrepancies between the obtained land surface temperatures (LSTs) and the air temperatures, together with information on the stations [27].

Table 3. Emissivity of representative terrestrial materials for LANDSAT 8 TIRS Band 10.

Terrestrial material	Water	Building	Soil	Vegetation
Emissivity	0.991	0.962	0.966	0.973

For this investigation, the mean NDVI value ranges from 0 to 0.2; hence, an emissivity value of 0.996 was applied. The formula for calculating emissivity (ε) is expressed using the Raster Calculator tool, and the procedure is executed accordingly.

$$\varepsilon = 0.004 * P_v + 0.986 \quad (8)$$

Determine Land Surface Emissivity (EM) utilizing the Fraction of Vegetation (FV). The 0.004 coefficient indicates the variance in emissivity attributable to vegetation, whereas the 0.986 denotes the baseline emissivity for other surfaces [28], [29].

Calculate the land surface temperature

The emissivity-corrected land surface temperatures (St) were computed as detailed below [22], [30]:

$$S_t = \frac{B_T}{1 + \left[\left(\frac{\lambda * B_T}{\rho}\right) * \ln \varepsilon_\lambda\right]} \quad (9)$$

where:

B_T = Top of atmosphere brightness temperature (K)

λ = wavelength of emitted radiance from Landsat-8 TIRS band 10 (λ = 10.895) [31] (Tables 4).

$$\rho = h\frac{c}{\sigma} = 1.4388 * 10^{-2} mK = 14388\ \mu K \quad (10)$$

h = Planck's constant = $6.626*10^{-34}$ J s

σ = Boltzmann constant = $1.38*10^{-23}$ J/K

c = velocity of light = $2.998*10^{8}$ m/s

Table 4: Wavelength of Landsat 8 TIRS bands 10 and 11.

Landsat 8 bands	Wavelength (micrometers)	Resolution (meters)
Band 10 - Thermal Infrared (TIRS) 1	10.60 - 11.19	100 (resampled to 30)
Band 11 - Thermal Infrared (TIRS) 2	11.50 - 12.51	100 (resampled to 30)

3. Results & Discussion

This study estimated LST values utilizing QGIS software and the 2024 Landsat 8 satellite picture of the Sarkoy district in Tekirdag province. In the computation of LST, NDVI was employed to assess the vegetation condition in 2024. NDVI is a vegetation technique utilized in environmental monitoring, capable of accurately

assessing plant state [32]. Figure 3 illustrates the NDVI fluctuations that delineate the regional distribution of vegetation quality in the research area for 2024.

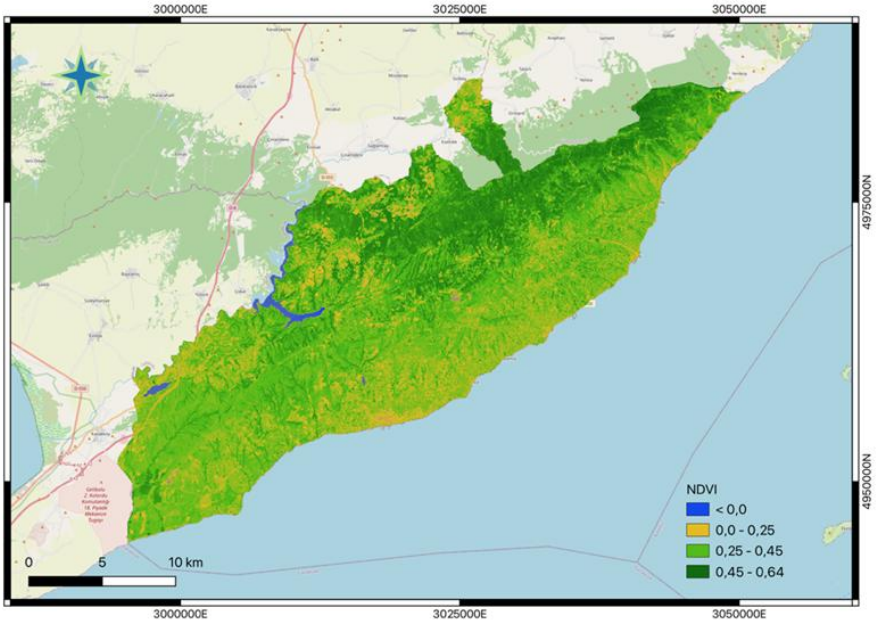

Figure 3: Spatial variations of NDVI in the research area

The land surface temperature (LST) was subsequently applied to all datasets. The spatial distributions of the The Land Surface Temperature (LST) derived from Landsat-8 OLI/TIRS on June 1, 2024, is illustrated in Figure 4. The distribution of LST in the research area on June 6, 2024, is illustrated. As a result of calculating the LST values, it is observed that the minimum is 19.678°C and the maximum is 37.289°C.

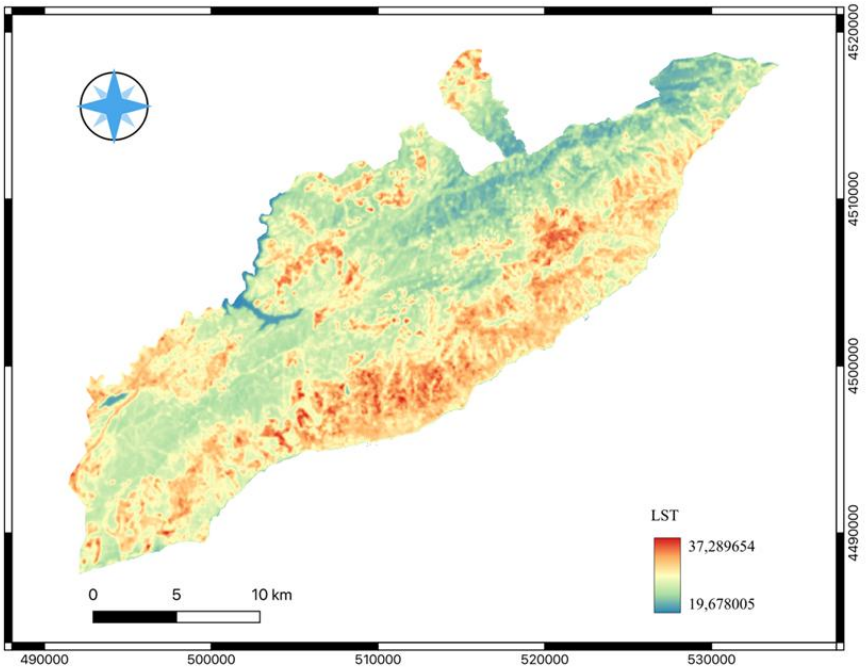

Figure 4: The LST variations of 2024 in Sarkoy region

A reclassification process was carried out to determine the area amounts covered by the distribution of LST values for the year 2024 in the Sarkoy district (fig.5). The calculated area values for the reclassified LST are also provided in Table 5 [31].

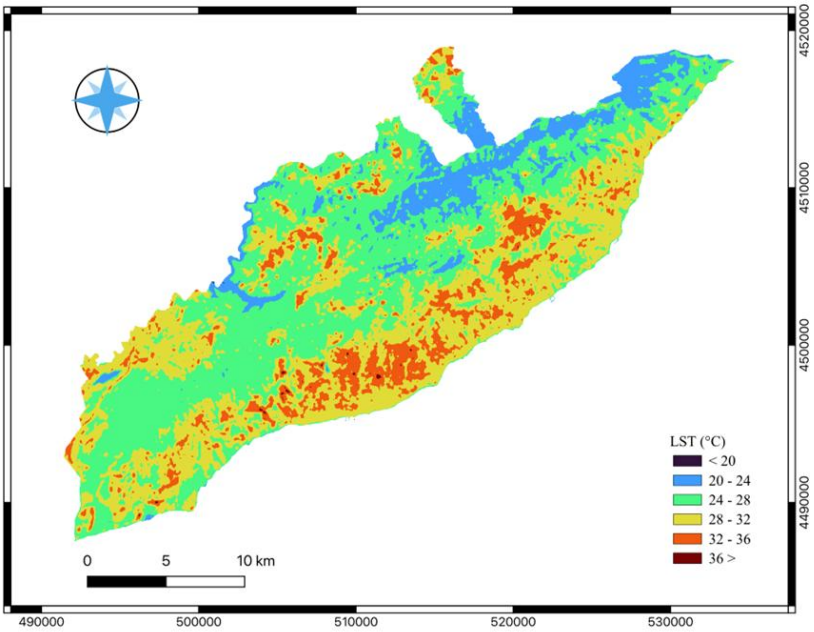

Figure 5: Reclassified spatial distributions of LST values.

Table 5: Reclassified geographical patterns of land surface temperature values.

LST (°C)	Area (m²)	Percentage (%)
< 20	2.07	0,004
22 – 24	5,230.71	10,137
24 – 28	22,475.88	43,557
28 – 32	19,039.50	36,898
32 – 36	4,813.29	9,328
36 >	39.06	0,076
Total	51,600.51	100.00

This research aims to determine the land surface temperature (LST) of the Sarkoy district based on the satellite-based Thermal infrared sensor of Landsat-8 OLI/TIRS. We found that the vegetation conditions on land surfaces identified by NDVI and LSE (ε) could trigger spatial variations in land surface temperature (LST).

The study may be informative for researchers regarding the impact of land use/cover on surface temperature under Sarkoy conditions. The results of this study can provide important information to researchers in agricultural topics, local administrators, and policymakers in determining the policies that should be adopted in future plans to address the growing populations of settlements and reduce increasing urban temperatures. Finally, the land surface temperature (LST) results from this study can be used to better understand the spatial variation in temperatures within the study area.

References

[1]. Mercan, Ç. (2020) Mardin Artuklu Üniversitesi, Savur Meslek Yüksekokulu, Harita ve Kadastro Programı, Mardin, Türkiye. Türkiye Uzaktan Algılama Dergisi – 2020; 2(2); 42-49.

[2]. Akyürek, Ö. (2020) Artvin Çoruh Üniversitesi, Doğal Afetler Uygulama ve Araştırma Merkezi. Doğal Afetler ve Çevre Dergisi- 2020; 6(2): 377-390.

[3]. Şekertekin, A., Kutoğlu, Ş. H., & Kaya, Ş. (2013). Uzaktan Algılama Verileri Yardımıyla Yer Yüzey Sıcaklığının Belirlenmesi. TMMOB Harita ve Kadastro Mühendisleri Odası, 14. Türkiye Harita Bilimsel ve Teknik Kurultayı, 14-17.

[4]. L. Chen, M. Li, F. Huang and S. Xu, (2013). Relationships of LST to NDBI and NDVI in Wuhan City based on Landsat ETM+ image, 2013 6th International Congress on Image and Signal Processing (CISP), Hangzhou, China, pp. 840-845.
[5]. Ermida, S. L., DaCamara, C. C., Trigo, I. F., Pires, A. C., Ghent, D., & Remedios, J. (2017). Modelling directional effects on remotely sensed land surface temperature. Remote Sensing of Environment, 190, 56-69.
[6]. Özkök, M. K., Tok, E., Gündoğdu, H. M., Demir, G. (2017) Kırklareli Üniversitesi, Mimarlık Fakültesi, Şehir ve Bölge Planlama Bölümü, Kırklareli. Toprak Bilimi ve Bitki Besleme Dergisi 5 (2) 69- 79.
[7]. Land Surface Temperature Technical Specification. (n.d.). Retrieved from https://developers.planet.com/docs/planetary-variables/land-surface-temperature-technical-specification/
[8]. Miralles, D. G., Holmes, T. R. H., De Jeu, R. A. M., Gash, J. H., Meesters, A. G. C. A., and Dolman, A. J. (2011). Global land-surface evaporation estimated from satellite-based observations, Hydrol. Earth Syst. Sci., 15, 453–469.
[9]. Intergovernmental Panel on Climate Change, Pirani, A., Connors, S. L., Péan, C., Berger, S., Caud, N., Zhou, B. (2021). Climate Change 2021: The Physical Science Basis. (V. Masson-Delmotte PhD & P. Zhai, Eds.), The Physical Science Basis. Retrieved from https://www.ipcc.ch/report/ar6/ wg1/ downloads/report/IPCC_AR6_WGI_SPM_final.pdf.
[10]. Merlin, O., Walker, J.P. Chehbouni, A., Kerr, Y., (2008). Towards deterministic downscaling of SMOS soil moisture using MODIS derived soil evaporative efficiency, Remote Sensing of Environment, Volume 112, Issue 10, Pages 3935-3946,
[11]. Mantey, S., Tagoe, N. D., & Abaidoo, C. A. (2014). Estimation of Land Surface Temperature and Vegetation Abundance Relationship – A Case Study. 3rd UMaT Biennial International Mining & Mineral Conference (p. 30th July-2nd August, 2014).
[12]. Voogt, J. A., & Oke, T. R. (2003). Thermal remote sensing of urban climates (journal-article). Remote Sensing of Environment (Vol. 86, pp. 370–384).
[13]. Xiao, R., Weng, Q., Ouyang, Z., Li, W., Schienke, E.W. and Zhang, Z. (2008) LandvSurface Temperature Variation and Major Factors in Beijing, China. Photogramm etric Engineering & Remote Sensing, 74, 451-461.
[14]. Franzpc. (2019, April 24). How to calculate Land Surface Temperature with Landsat 8 satellite images. Retrieved from https://giscrack.com/how-to-calculate-land-surface-temperature-with-landsat-8-images/
[15]. Twumasi, Y. A., Merem, E. C., Namwamba, J. B., Mwakimi, O. S., Ayala-Silva, T., Frimpong, D. B., Mosby, H. J. (2021). Estimation of Land Surface Temperature from Landsat-8 OLI Thermal Infrared Satellite Data. A Comparative Analysis of Two Cities in Ghana. Advances in Remote Sensing, 10 (04), 131–149.
[16]. Albut, S., Uysal, T., Namık Kemal University, & Tekirdag Viticultural Research Institute. (2010). The Determination of The Alteration of Vineyards in Tekirdağ and Evaluation of Topographicly Appropriate Vineyard Areas in Tekirdağ -Şarköy District by Geographic Information Systems (GIS).
[17]. U.S. Geological Survey (2024a) EarthExplorer-Home. Satellite Data. https://earthexplorer.usgs.gov/
[18]. U.S. Geological Survey (2024b) Landsat Missions: Using the USGS Landsat Level-1 Data Product. https://www.usgs.gov/landsat-missions/using-usgs-landsat-level-1-data-product .
[19]. Marino, F. (2024, November 19). Top of Atmosphere Reflectance on Sentinel 3. Retrieved from https://www.earthstartsbeating.com/2017/04/27/top-of-atmosphere-reflectance-on-sentinel-3/#:~:text=Top%20of%20Atmosphere%20(TOA)%20Reflectance,and%20the%20solar%20zenith%20angle
[20]. Aman, A., Randriamanantena, H.P., Podaire, A. and Froutin, R. (1992) Upscale Integration of Normalized Difference Vegetation Index: The Problem of Spatial Heterogeneity. IEEE Transactions on Geoscience and Remote Sensing, 30, 326-338.

[21]. Rouse, J.W., Haas, R.W., Schell, J.A., Deering, D.W. and Harlan, J.C. (1974) Monitoring the Vernal Advancements (Greenwave Effect) and Retrogradation of Natural Vegetation. NASA/GSFCT Type III Final Report, Texas A & M University, Remote Sensing Center, College Station, 1-137.

[22]. Weng, F., Qin, Z., Song, C., Tu, L., Karnieli, A., & Zhao, S. (2004). An Improved Mono-Window Algorithm for Land Surface Temperature Retrieval from Landsat 8 Thermal Infrared Sensor Data. Remote Sensing, c7(4), 4268–4289

[23]. Tutorial: Estimation of Land Surface Temperature with Landsat and ASTER — Τεκμηρίωση του Semi-Automatic Classification Plugin - 5.3.6.1. (n.d.). Retrieved from https://semiautomaticclassification manual-v5.readthedocs.io/ el/latest/thematic_tutorial_temperature.html

[24]. Jimenez-Munoz, J.C., Sobrino, J.A., Gillespie, A., Sabol, D. and Gustafson, W.T. (2006) Improved Land Surface Emissivities over Agricultural Areas Using ASTER NDVI. Remote Sensing of Environment, 103, 474-487.

[25]. Sobrino, J.A., Jiménez-Muñoz, J.C. and Paolini, L. (2004) Land Surface Temperature Retrieval from LANDSAT TM5. Remote Sensing of Environment, 90, 434-440.

[26]. Sobrino, J.A. and Raissouni, N. (2000) Toward Remote Sensing Methods for Land Cover Dynamic Monitoring: Application to Morocco. International Journal of Remote Sensing, 21, 353-366.

[27]. Avdan, U., & Jovanovska, G. (2016). Algorithm for Automated Mapping of Land Surface Temperature Using LANDSAT 8 Satellite Data. Journal of Sensors, 2016, 1–8.

[28]. Ridho, M. (2024, June 8). Analyzing Land Surface Temperature (LST) with Landsat 8 Data in Google Earth Engine. Medium. Retrieved from https://medium.com

[29]. Li, Z., Wu, H., Wang, N., Qiu, S., Sobrino, J. A., Wan, Z., . . . Yan, G. (2012). Land surface emissivity retrieval from satellite data. International Journal of Remote Sensing, 34(9–10), 3084–3127.

[30]. Saha, J., Ria, S. S., Sultana, J., Shima, U. A., Seyam, M. M. H., & Rahman, M. M. (2023). Assessing seasonal dynamics of land surface temperature (LST) and land use land cover (LULC) in Bhairab, Kishoreganj, Bangladesh: A geospatial analysis from 2008 to 2023. Case Studies in Chemical and Environmental Engineering, 9, 100560.

[31]. Sholihah, R. I., & Shibata, S. (2019). Retrieving Spatial Variation of Land Surface Temperature Based on Landsat OLI/TIRS: A Case of Southern part of Jember, Java, Indonesia. IOP Conference Series Earth and Environmental Science, 362(1), 012125.

[32]. B. Adamu, K. Tansey and B. Ogutu, "Remote sensing for detection and monitoring of vegetation affected by oil spills," International Journal of Remote Sensing, vol. 39(11), pp. 3628-3645, 2018.